

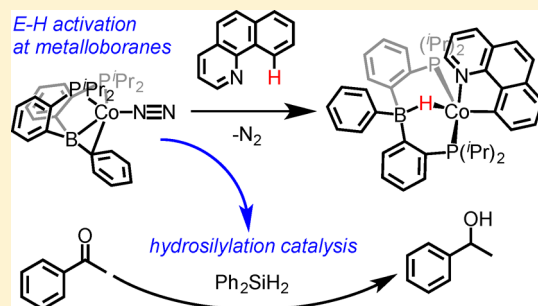
E–H Bond Activations and Hydrosilylation Catalysis with Iron and Cobalt Metalloboranes

Mark A. Nesbit, Daniel L. M. Suess, and Jonas C. Peters*

Division of Chemistry and Chemical Engineering, California Institute of Technology, 1200 East California Boulevard, Pasadena, California 91125, United States

S Supporting Information

ABSTRACT: An exciting challenge in transition metal catalyst design is to explore whether earth-abundant base metals such as Fe, Co, and Ni can mediate two-electron reductive transformations that their precious metal counterparts (e.g., Ru, Rh, Ir, and Pd) are better known to catalyze. Organometallic metalloboranes are an interesting design concept in this regard because they can serve as organometallic frustrated Lewis pairs. To build on prior studies with nickel metalloboranes featuring the DPB and ^{Ph}DPB^{Mes} ligands in the context of H₂ and silane activation and catalysis (DPB = bis(*o*-diisopropylphosphinophenyl)phenylborane, ^{Ph}DPB^{Mes} = bis(*o*-diphenylphosphinophenyl)mesitylborane), we now explore the reactivity of iron, [(DPB)Fe]₂(N₂), **1**, and cobalt, (DPB)Co(N₂), **2**, metalloboranes toward a series of substrates with E–H bonds (E = O, S, C, N) including phenol, thiophenol, benzo[*h*]quinoline, and 8-aminoquinoline. In addition to displaying high stoichiometric E–H bond activation reactivity, complexes **1** and **2** prove to be more active catalysts for the hydrosilylation of ketones and aldehydes with diphenylsilane relative to (^{Ph}DPB^{Mes})Ni. Indeed, **2** appears to be the most active homogeneous cobalt catalyst reported to date for the hydrosilylation of acetophenone under the conditions studied.



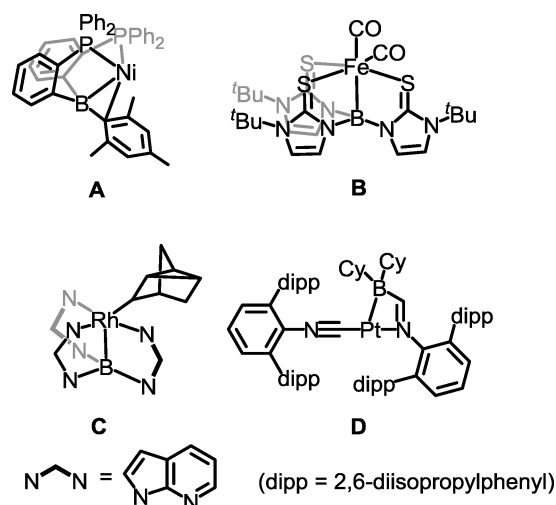
INTRODUCTION

The ability of transition metals to mediate multielectron transformations is critical in organometallic catalysis. Noble metals are prominent in organometallic catalysis due to their tendency to display well-defined multielectron reactivity.¹ E–H bond oxidative additions and reductive eliminations are key steps in many of these catalytic processes, such as olefin hydrogenation and the hydrosilylation of ketones and aldehydes.^{2–4} There has been increasing interest in developing well-defined complexes featuring earth-abundant first-row transition metals that can mediate similar two-electron redox steps and thus serve as viable catalysts for these types of transformations.^{5,6}

One promising strategy for imparting nobility to first-row transition metal systems is the use of ligands that incorporate a pendant borane.^{7–11} The weak or labile interaction between the transition metal center and the boron atom in the ligand can be considered as an organometallic frustrated Lewis pair wherein the pendant borane formally serves as the Lewis acid and an electron-rich, low-valent metal center serves as the Lewis base.^{9–14} This point was highlighted by our lab in recent studies of the reactivity of a nickel metalloborane (^{Ph}DPB^{Mes})Ni (Chart 1, A) with hydrogen.⁹ This limiting polarity is inverted from the more typical case where a Lewis acidic metal is paired with a ligand featuring a Lewis basic site.^{5,8,9,15,16}

Other metalloborane platforms have also been shown to facilitate oxidative additions across the metal–borane interaction. For instance, Parkin and co-workers showed that Fe and

Chart 1. Select Metal–Borane Compounds That Facilitate Bond Activations via Cleavage of the M–B Interaction



Ni compounds supported by a tris(mercaptoimidazolyl)borane ligand (e.g., (B(mim^{tBu})₃)Fe(CO)₂, Chart 1, B) facilitate 1,2-addition of a variety of E–X bonds across the transition metal–

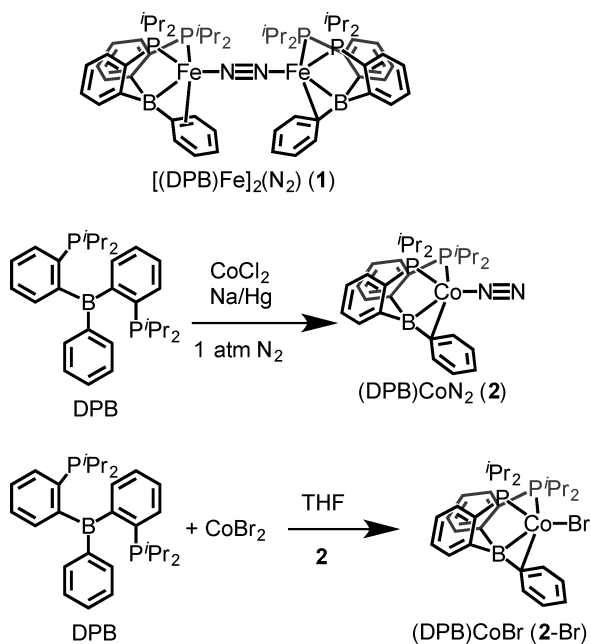
Special Issue: Gregory Hillhouse Issue

Received: June 18, 2015

borane interaction.^{17,18} Related to our own studies of nickel metalloboranes, Owen and co-workers demonstrated that the rhodium compound Rh[B(azaindoyl)₃](nortricyclyl) (Chart 1, C) facilitates oxidative addition of H₂ and serves as an olefin hydrogenation catalyst.¹⁹ Very recently, Emslie and Figueroa have independently reported platinum compounds bearing a pendant borane that activate H₂ and other E–H bonds (Chart 1, D).^{20,21}

Stimulated by these recent advances that show M–B dative interactions can facilitate well-defined multielectron chemistry at base metal centers, we now describe the reactivity of the Fe and Co metalloboranes [(DPB)Fe]₂(N₂), **1**, and (DPB)Co(N₂), **2** (Scheme 1). We report here a comparative study on the

Scheme 1. M–N₂ Adducts **1** and **2**



reactivity of **1** and **2** in the context of E–H bond activation and catalytic hydrosilylation of ketones and aldehydes, and compare their activity to the Ni analogue (Chart 1, A), which has been previously demonstrated to be a competent catalyst for olefin hydrogenation and benzaldehyde hydrosilylation.^{9,11} Ultimately, we find that **1** and **2** display enhanced reactivity profiles toward E–H bonds by comparison to the aforementioned Ni system and that **2** serves as a very active precatalyst for the hydrosilylation of organic carbonyls. Furthermore, we have independently prepared several efficient hydrosilylation catalysts reported in the literature^{22–24} to test them against **1** and **2** and have found **2** to be the most active cobalt precatalyst under the conditions described herein.

RESULTS AND DISCUSSION

We have previously described the synthesis of [(DPB)Fe]₂(N₂) (Scheme 1, **1**)²⁵ and have reported Si–H and H–H bond activations by related iron compounds derived from silylation of bound N₂ and CO.^{25,26} A cobalt analogue, (DPB)Co(N₂) (Scheme 1, **2**), has been synthesized for this study to compare with **1**. A solution magnetic susceptibility measurement of **2** (1.8 μ_B at rt) is consistent with an S = 1/2 ground state. The presence of a terminally bound N₂ ligand was supported by X-ray crystallographic studies (Figures 1, 2, and S1), which

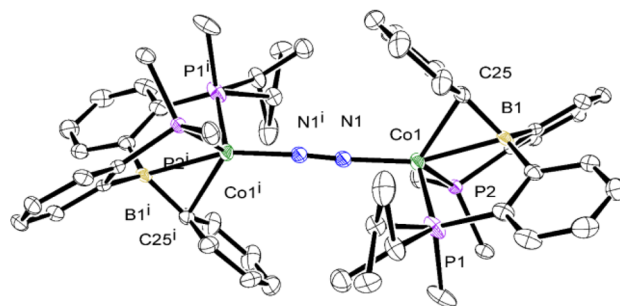


Figure 1. ORTEP representation of the N₂-bridged dimer generated by inversion symmetry in the solid-state structure of **2**. Selected bond distances (Å): Co1–P1 2.2754(9); Co1–P2 2.2890(8); Co1–N1 1.900(2); Co1–B1 2.282(3); Co1–C25 2.113(3). One of the isopropyl groups on P1 is disordered over two positions.

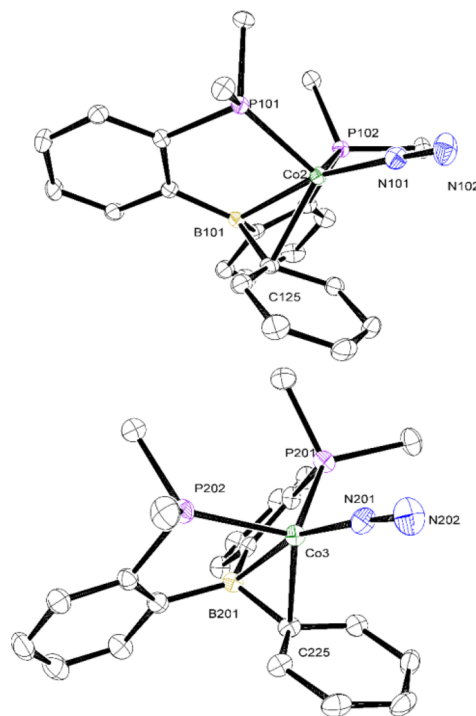


Figure 2. ORTEP representations of terminal N₂ adducts from the asymmetric unit of **2** (H atoms and methyl groups on nondisordered isopropyl substituents are omitted for clarity). Selected bond distances (Å): Co2–P102 2.2594(8); Co2–P101 2.2616(8); Co2–N101 1.845(2); Co2–C125 2.099(2); Co2–B101 2.240(3); Co3–P201 2.2645(8); Co3–P202 2.2607(9); Co3–N201 1.846(2); Co3–C225 2.054(3); Co3–B201 2.225(3).

showed the presence of two (DPB)Co(N₂) molecules and an N₂-bridged dimer ([[(DPB)Co]₂(N₂)) in the asymmetric unit; the nickel derivative (DPB)Ni(N₂) behaves similarly in the solid state.¹⁵ ATR-FTIR and solution IR spectra showed intense N₂ stretching bands at 2098 cm^{−1}, establishing the terminal N₂ adduct as the major species in solution.

Reactivity with PhOH and PhSH. Addition of PhOH (2 equiv) to **1** in C₆D₆ results in formation of an unusual Fe(I) terminal phenolate adduct, (DPB)Fe(OPh), **1a**, with concomitant release of H₂ (detected by GC; Scheme 2). Compound **1a** is an S = 3/2 paramagnet with a solution magnetic moment of 3.9 μ_B (C₆D₆, 25 °C). The Fe–P_{av} and Fe–B distances of 2.38 and 2.340(3) Å in **1a** determined by X-ray crystallographic studies (Figure 3) are similar to those observed in the

Scheme 2. E–H Bond Activations Mediated by 1

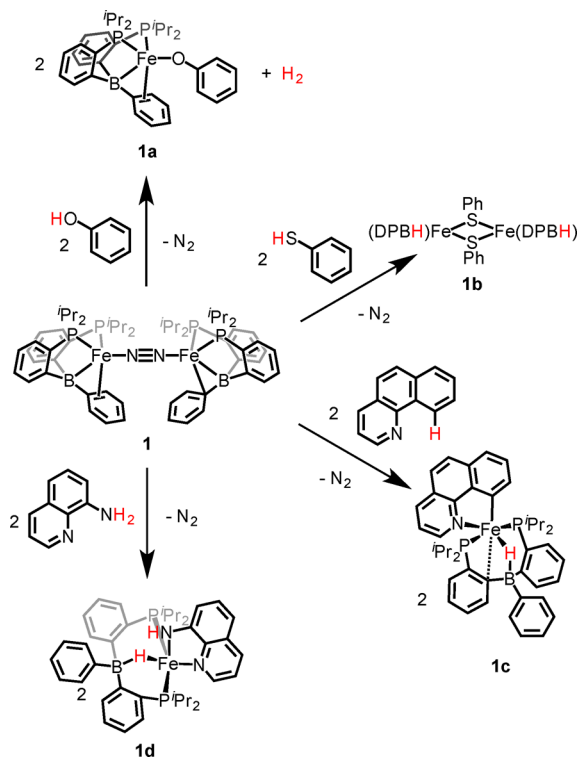


Figure 3. Solid-state structure of **1a**. Thermal ellipsoids are drawn at the 50% probability level. Methyl substituents on the isopropyl groups and hydrogen atoms attached to carbon have been omitted for clarity. Selected bond distances for **1a** (Å): Fe–P1, 2.3736(7); Fe–P2, 2.3777(6); Fe–B, 2.340(3); Fe–O, 1.8665(18); Fe–C7, 2.237(2); Fe–C8, 2.434(3).

previously reported $S = 3/2$ (DPB)FeBr (Fe– P_{av} = 2.38 Å, Fe–B = 2.3242(11) Å, μ_{eff} = 3.8 μ_B).²⁵ This fact further supports the formulation of **1a** as a high-spin Fe(I) phenolate. In contrast, addition of PhSH to **1** gives the dimeric Fe(II) borohydride-phenylthiolate adduct [(DPBH)Fe(SPh)]₂, **1b**, resulting from formal S–H bond oxidative addition. The ATR-FTIR of **1b** shows a broad absorbance centered at 1949 cm^{-1} that is consistent with the presence of a B–H–Fe moiety.^{25,26} Additionally, the solid-state structure of **1b** shows the absence of a metal–arene interaction and an elongated Fe–B distance of 3.019(2) Å (Figure 4) versus 2.3739(7) and 2.3136(7) Å in **1**.^{25,27}

Treatment of **2** with PhOH or PhSH gave the isostructural phenolate and phenylthiolate adducts (DPB)Co(OPh), **2a** (μ_{eff} = 3.2 μ_B at 25 °C), and (DPB)Co(SPh), **2b** (μ_{eff} = 2.6 μ_B at 25 °C), respectively (Scheme 3), accompanied by the release of H₂ (detected by GC). The solid-state structures of **2a** and **2b** are

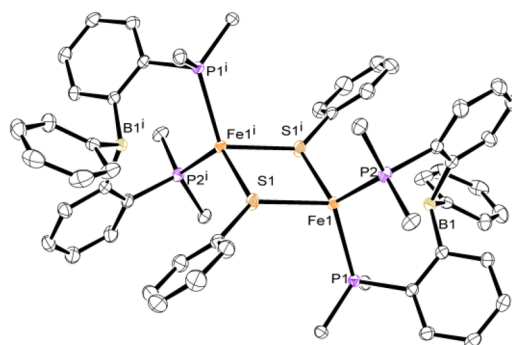
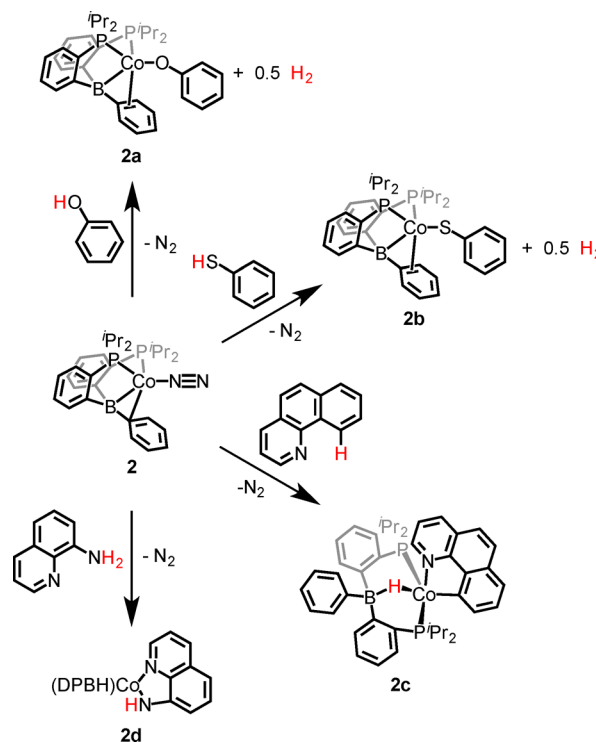


Figure 4. Solid-state structure of **1b**. Thermal ellipsoids are drawn at the 50% probability level. Methyl substituents on the isopropyl groups and hydrogen atoms attached to carbon have been omitted for clarity. Selected distances for **1b** (Å): Fe–P1, 2.49770(13); Fe–P2, 2.5296(2); Fe–B, 3.019(2); Fe–S1, 2.42445(18); Fe–S1', 2.37283(14).

Scheme 3. E–H Bond Activations Mediated by 2



shown in Figure 5 and Figure 6. The Co–O distance of 1.8904(15) Å in **2a** (Figure 5) is consistent with the only other structurally characterized Co(I) compound bearing a terminal phenolate ligand, (PPh₃)₃CoOPh; the latter species displays a Co–O distance of 1.9 Å.²⁸ Other Co(II) compounds bearing a terminal phenolate ligand have similar Co–O distances ranging from 1.85 to 1.91 Å.^{29,30} Terminal Co(I) phenylthiolate compounds are more common, and the observed Co–S distance of 2.2483(3) Å in **2b** lies within the reported range 2.24–2.35 Å.^{31–35} Furthermore, the Co– P_{av} distances of 2.29 Å for **2a** and 2.33 Å for **2b** and the Co–B distances of 2.302(2) Å for **2a** and 2.2828(12) Å for **2b** closely match the Co– P_{av} distance of 2.30 Å and Co–B distance of 2.3070(7) Å in **2-Br** (Figure S2). Additional confirmation of the identities of compounds **1a**, **2a**, and **2b** was obtained by independent

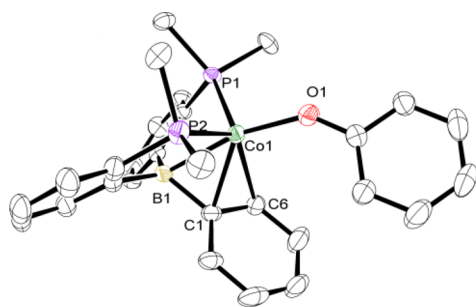


Figure 5. Solid-state structure of **2a**. Thermal ellipsoids are drawn at the 50% probability level. Methyl groups on the isopropyl substituents and hydrogen atoms bonded to carbon have been omitted for clarity. Selected distances for **2a** (Å): Co–P1, 2.2984(5); Co–P2, 2.2813(6); Co–B, 2.302(2); Co–O, 1.8904(15); Co–C1, 2.245(2); Co–C6, 2.499(2).

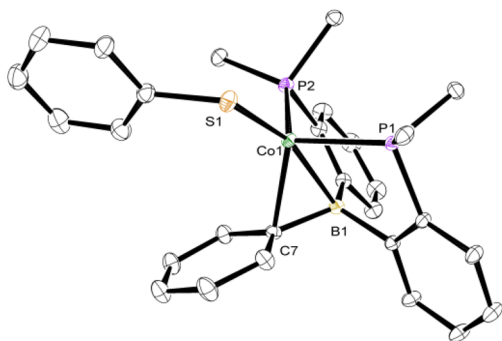


Figure 6. Solid-state structure of **2b**. Thermal ellipsoids are drawn at the 50% probability level. Methyl groups on the isopropyl substituents and hydrogen atoms bonded to carbon have been omitted for clarity. Selected distances for **2b** (Å): Co–P1, 2.3381(3); Co–P2, 2.3203(3); Co–B, 2.2828(12); Co–S, 2.2483(3); Co–C7, 2.2390(11).

preparation of **1a**, **2a**, and **2b** from the reaction of (DPB)FeBr or **2-Br** with NaOPh or NaSPh in THF.

Reactivity of 1 and 2 with Benzo[*h*]quinolone. Compounds **1a**, **2a**, and **2b** can be considered as the products of formal one-electron processes in which **1** or **2** acts as a reductant. One plausible mechanistic scenario that could lead to products such as **1a**, **2a**, and **2b** is where a four-coordinate Fe(II) or Co(II) borohydride-phenolate or a Co(II) borohydride-phenylthiolate is transiently formed. This transient could then be followed by a bimolecular reductive elimination step to release H₂ and generate the observed monovalent products. While we have not undertaken mechanistic studies of the reactions that produce **1a**, **2a**, and **2b**, the isolation of **1b** suggested species of this type might be more generally accessible. The structure of **1b** also indicated that a species formed by oxidative addition of an E–H bond at **1** or **2** might be stabilized by increasing the coordination number of the metal center to five. With this in mind, we explored the reactivity of **1** and **2** with chelating substrates that could stabilize the products of E–H bond oxidative addition.

Benzo[*h*]quinolone has been used previously as a substrate in directed C–H bond arylation.^{36–38} Heating benzo[*h*]quinoline with **1** in benzene to 70 °C for a period of ca. 3 h cleanly afforded the oxidative addition product (DPBH)Fe(benzo[*h*]quinolin-10-yl), **1c** (Scheme 2). Complex **1c** adopts a six-coordinate structure in the solid state and is diamagnetic (Figure 7). A broad singlet appears in its ¹H NMR spectrum located at $\delta = -22.80$ ppm, consistent with a borohydride. The

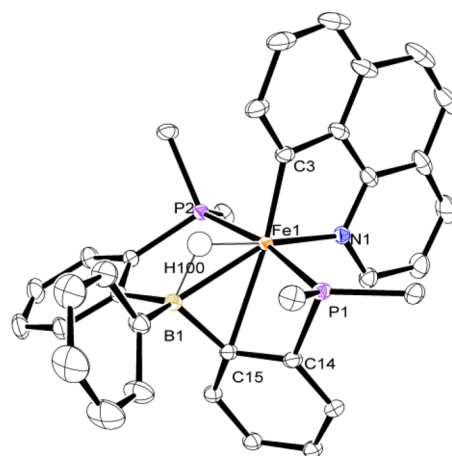


Figure 7. Solid-state structures of **1c**. Thermal ellipsoids are drawn at the 50% probability level. Methyl substituents on the isopropyl groups and hydrogen atoms bonded to carbon have been omitted for clarity. Selected distances for **1c** (Å): Fe–P1, 2.2189(3); Fe–P2, 2.2665(3); Fe–H100, 1.591(19); Fe–C3, 1.9286(8); Fe–N1, 1.9682(8); Fe–C15, 2.3739(8); Fe–B, 2.3342(9).

bridging B–H–Fe moiety was confirmed via an XRD study, and the bridging hydride was successfully located and refined (Figure 7). The Co analogue (DPBH)Co(benzo[*h*]quinolin-10-yl), **2c** (Scheme 3), was synthesized under similar conditions and is an $S = 1/2$ paramagnetic species with a solution magnetic moment of 1.79 μ_B (C₆D₆, 25 °C). Complex **2c** displays a broad M–H–B stretch at 2047 cm^{−1} in its thin-film ATR-FTIR spectrum.

Interestingly, the Fe center in **1c** interacts with one of the *ipso* carbons on the borane ligand to adopt a distorted octahedral geometry resulting in an 18-electron, $S = 0$ ground state (Figure 7). In contrast **2c** adopts a five-coordinate geometry best described as a distorted square-based pyramid ($\tau_5 = 0.386$) (Figure 6; $\tau_5 = 0$ for ideal square-based pyramid, $\tau_5 = 1$ for ideal trigonal bipyramid)³⁹ to give the observed 17-electron, $S = 1/2$ ground state (Figure 8).

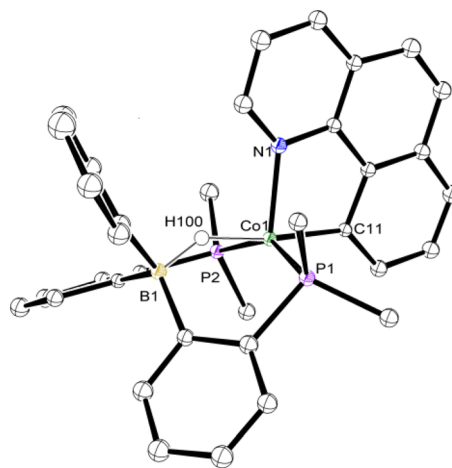


Figure 8. Solid-state structure of **2c**. Thermal ellipsoids are drawn at the 50% probability level. Methyl substituents on the isopropyl groups and hydrogen atoms bonded to carbon have been omitted for clarity. Selected distances for **2c** (Å): Co–P1, 2.2604(18); Co–P2, 2.2331(18); Co–H100, 1.59(5); Co–N1, 2.040(5); Co–C11, 1.931(6); Co–B, 2.698.

Reactivity of 1 and 2 with 8-Aminoquinoline. N–H bond activation and functionalization using Fe and Co is less well established than C–H activation. Reports of N–H bond activation with Fe are primarily limited to relatively acidic amides,^{40,41} and N–H bond activation chemistry of amines by Co is similarly scarce.^{42–45} The N–H bond in 8-aminoquinoline adds across the M–B unit in 1 and 2 to afford (DPBH)Fe(8-amidoquinoline), 1d, and (DPBH)Co(8-amidoquinoline), 2d over several hours at room temperature (Schemes 2 and 3). In the case of 2d the reaction reaches completion more quickly by evacuating the head space via freeze–pump–thaw cycles to remove N₂.

The ¹H NMR spectrum of the reaction mixture producing 1d shows more than 30 paramagnetically broadened and shifted peaks, suggesting either a single species with C₁ symmetry in solution or two different C_s symmetric species. The distribution of products does not change when the reaction is run at elevated temperatures (80 °C), and the ¹H NMR spectrum of the reaction mixture in d₈-toluene does not change significantly over the temperature range of 25 to 75 °C. Cooling to low temperatures (–90 °C) results in the disappearance of most of the paramagnetically shifted features with no new diamagnetic signals (Figure S3). Single crystals of the reaction products were highly twinned in many cases; the least twinned crystal of several screened was chosen and showed the anticipated N–H oxidative addition product 1d with the major component (~90%) having the amido group located *cis* to the borohydride and the minor component (~10%) having the amido group *trans* to the borohydride (Figures 9 and 10). The bond metrics

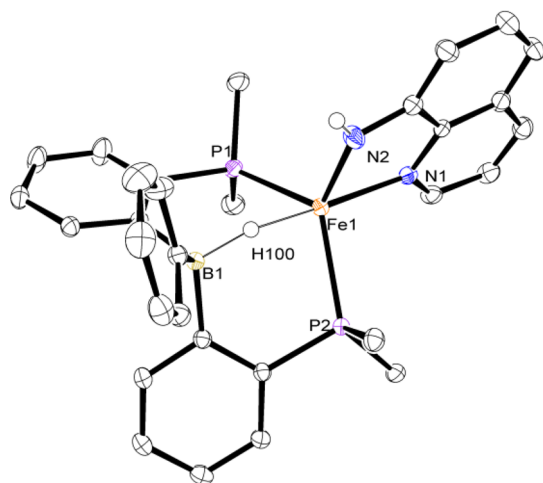


Figure 9. Solid-state structure of the major component (90%) of a twinned crystal of 1d. Ellipsoids are drawn at the 50% probability level. Methyl substituents on the isopropyl groups and hydrogen atoms bonded to carbon have been omitted for clarity. Selected distances for the major component of 1d (Å): Fe–P1, 2.4324(5); Fe–P2, 2.4552(5); Fe–H100, 1.77(2); Fe–N1, 2.1920(15); Fe–N2, 1.9584(19); Fe–B, 2.9667(17).

of the major component showed a borohydride moiety and elongated Fe–P distances indicative of an *S* = 2 species (Figure 9). This assignment is supported by the solution magnetic moment of 5.2 μ_B (C₆D₆, 25 °C), which is consistent with the presence of high-spin Fe(II) isomers of the appropriate molecular weight. The high-spin ground state observed for 1d is interesting since the similar C–H activation product 1c is diamagnetic. The difference in spin states is also reflected in the

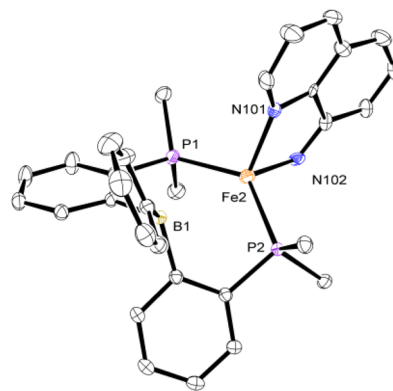


Figure 10. Solid-state structure of the minor component (10%) of a twinned crystal of 1d. Ellipsoids are drawn at the 50% probability level. Methyl substituents on the isopropyl groups and hydrogen atoms bonded to carbon have been omitted for clarity.

solid-state structure (Figure 9) of 1d; it adopts a five-coordinate distorted trigonal bipyramid geometry ($\tau_5 = 0.82$) as opposed to the six-coordinate pseudo-octahedral geometry observed in 1c. This difference in geometry is presumably due to the weaker ligand field exerted by the amido ligand compared to the aryl ligand. As a result, the Fe–H distance in 1d lengthens relative to that in 1c. Evidence in support of this idea can be found in the IR spectrum of 1d, which shows intense but broad absorptions at 2130 and 2000 cm^{–1} corresponding to B–H–Fe stretches in the two conformational isomers. It remains unclear as to whether formation of the two isomers observed is due to conversion between the two conformations after the N–H bond activation step or if their formation results from differing N–H bond activation pathways.

Reaction of 2 with 8-aminoquinoline proceeds similarly with formation of dark purple (DPBH)Co(8-amidoquinoline), 2d, after stirring at room temperature for about 16 h. While single crystals of sufficient quality for X-ray diffraction studies could not be obtained, the proposed connectivity was inferred from the IR spectrum of 2d, which shows a broad B–H–Co stretch at 1961 cm^{–1} and weaker broad N–H stretches at 3384 and 3478 cm^{–1}. Additionally, the 77 K frozen solution X-band EPR spectra of 2c and 2d are very similar and suggest similar geometries and spin states at the cobalt center (see Figures S4 and S5 in the Supporting Information). Combustion analysis data are also consistent with this formulation.

Reactivity of (DPB)Co(N₂) with Diphenylsilane. The addition of Ph₂SiH₂ to 1 gave a mixture of unidentified products. Addition of 1 equiv of Ph₂SiH₂ to 2 at room temperature under an atmosphere of N₂ resulted in partial consumption of 2 and formation of a small amount of a new paramagnetic species as judged by ¹H NMR spectroscopy (Figure 11, spectrum A). Upon addition of excess Ph₂SiH₂ (10 equiv), a new species with paramagnetically shifted resonances can be clearly observed, although 2 is still present (Figure 11, spectrum B). Increasing the amount of Ph₂SiH₂ to 100 equiv shows an increase in the concentration of the new paramagnet relative to 2 (Figure 11, spectrum C). Subjecting the reaction mixture to three freeze–pump–thaw cycles drives complete conversion of 2 into the new species (Figure 11, spectrum D). Reintroduction of N₂ to the J-Young NMR tube followed by stirring overnight regenerates the spectrum shown in Figure 11C. These observations suggest that an equilibrium between (DPB)Co(N₂) and the new species observed by ¹H NMR

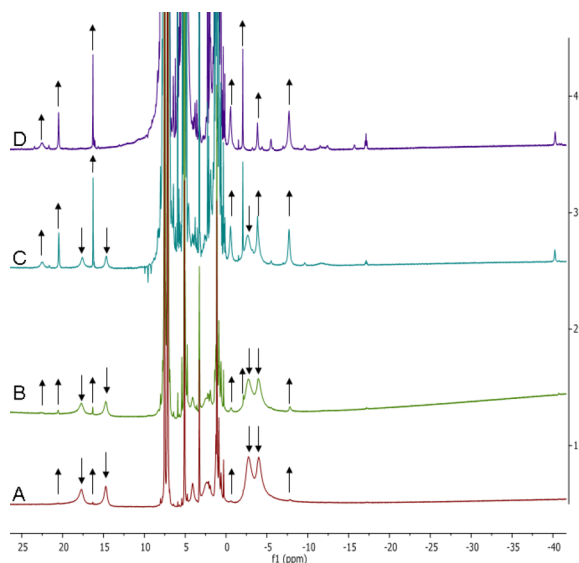
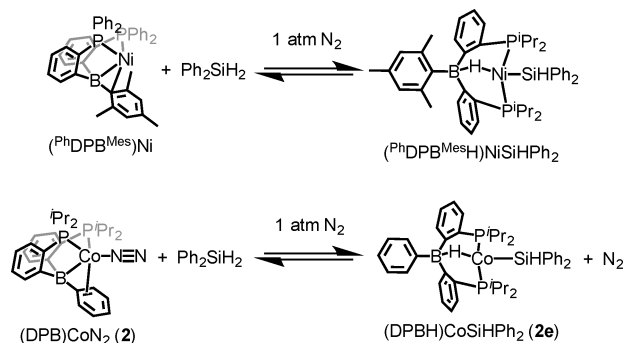


Figure 11. ^1H NMR spectra in C_6D_6 of **2** in the presence of Ph_2SiH_2 under N_2 (A–C) and vacuum (D). (A) **2** + 1 equiv of Ph_2SiH_2 . (B) **2** + 10 equiv of Ph_2SiH_2 . (C) **2** + 100 equiv of Ph_2SiH_2 . (D) **2** + 100 equiv of Ph_2SiH_2 under vacuum. Upward arrows indicate the new paramagnetic species growing in assigned as $(\text{DPBH})\text{Co}(\text{SiHPh}_2)$, **2e**. Downward arrows indicate consumption of **2**.

spectroscopy (formulated as $(\text{DPBH})\text{Co}(\text{SiHPh}_2)$, **2e**) exists, as was observed for $(^{\text{Ph}}\text{DPB}^{\text{Mes}})\text{Ni}$ and $(^{\text{Ph}}\text{DPB}^{\text{Mes}}\text{H})\text{Ni}(\text{SiHPh}_2)$ (Scheme 4).¹¹ A small amount of an unidentified

Scheme 4. Reversible Si–H activation at $(^{\text{Ph}}\text{DPB}^{\text{Mes}})\text{Ni}$ and **2**



diamagnetic Co side-product was also observed in the ^1H NMR spectrum, which displays a triplet resonance centered at -17.13 ppm with $^2J_{\text{P-H}} = 44.3$ Hz.

The reaction of **2** with 100 equiv of Ph_2SiH_2 was studied by X-band EPR spectroscopy at 77 K in benzene under vacuum in order to gain further characterization of **2e**. Upon degassing the reaction mixture with three freeze–pump–thaw cycles, a slight color change from red–orange to orange was observed and the ^1H NMR spectrum of the reaction mixture confirmed complete consumption of **2** (Figure 11 spectrum D). The EPR spectrum of the reaction mixture (Figure 12) showed clean formation of a new $S = 1/2$ species, which arises from the new paramagnetic species observed in the ^1H NMR: $(\text{DPBH})\text{Co}(\text{SiHPh}_2)$, **2e** (Figure 11). To support the assignment of $(\text{DPBH})\text{Co}(\text{SiHPh}_2)$, **2e**, we conducted solution IR studies of **2** in the presence of 100 equiv of diphenylsilane under a nitrogen atmosphere. Under these conditions a feature at 1810 cm^{-1} was

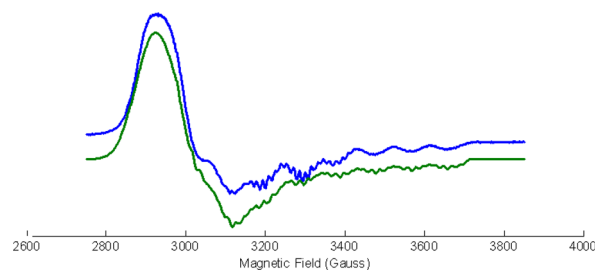


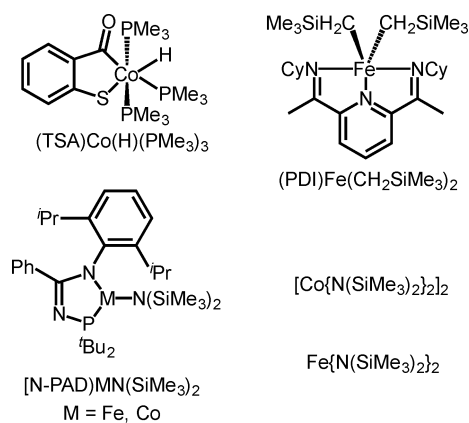
Figure 12. X-Band EPR spectrum of $(\text{DPBH})\text{Co}(\text{SiHPh}_2)$, **2e**, in benzene at 77 K (9.49 GHz) (top, blue trace) and simulation (bottom, green trace) ($g_1 = 2.2836$, $g_2 = 2.1703$, $g_3 = 2.0098$; nuclei = Co, P, P, H; $A_{\text{Co}} = 255.346$ MHz, $A_{\text{P1}} = 111$ MHz, $A_{\text{P2}} = 62$ MHz, $A_{\text{H}} = 39$ MHz; $\text{HStrain}_1 = 275.565$ MHz, $\text{HStrain}_2 = 375.565$ MHz, $\text{HStrain}_3 = 35$ MHz).

observed, which can be assigned to a B–H–Co stretching mode.

Catalytic Hydrosilylation of Ketones and Aldehydes.

We next explored the activity of **1** and **2** as precatalysts for the hydrosilylation of organic carbonyl compounds and compared their activity to that of $(^{\text{Ph}}\text{DPB}^{\text{Mes}})\text{Ni}$.^{9,11} The ability of transition metal compounds to facilitate catalytic hydrosilylation of ketones and aldehydes has been highlighted for synthetic methodological significance relative to stoichiometric reductants (e.g., LiAlH_4), and the hydrosilylation of carbon–oxygen multiple bonds has been targeted in the context of organic substrate functionalizations and catalytic CO_2 and CO reduction.^{46–55} A number of groups have thus targeted first-row transition metal catalysts including iron and cobalt to this end.^{22–24,49,56–64} A selection of the most efficient reported iron and cobalt hydrosilylation catalysts is shown in Chart 2.

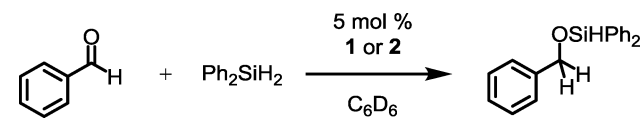
Chart 2. Selected Examples of Previously Reported Fe and Co Carbonyl Hydrosilylation Catalysts



Precatalysts **1** and **2** were tested under our previously reported conditions for the catalytic hydrosilylation of benzaldehydes.¹¹ Both **1** and **2** are far more active catalysts than $(^{\text{Ph}}\text{DPB}^{\text{Mes}})\text{Ni}$, consistent with their higher degree of reactivity toward E–H bonds relative to $(^{\text{Ph}}\text{DPB}^{\text{Mes}})\text{Ni}$. Full consumption of benzaldehyde was achieved in under 2 min in both cases, while the previously reported $(^{\text{Ph}}\text{DPB}^{\text{Mes}})\text{Ni}$ system required several hours to reach completion (Table 1).

The previously reported $(^{\text{Ph}}\text{DPB}^{\text{Mes}})\text{Ni}$ benzaldehyde hydrosilylation system showed rate enhancement with electron-donating groups, contrasting Chirik's $(\text{PDI})\text{Fe}(\text{CH}_2\text{SiMe}_3)_2$ system and other carbonyl reduction catalysts, which have

Table 1. Comparison of **1** and **2** to $(\text{Ph}^{\text{DPB}}\text{Mes})\text{Ni}$ for Benzaldehyde Hydrosilylation by Ph_2SiH_2

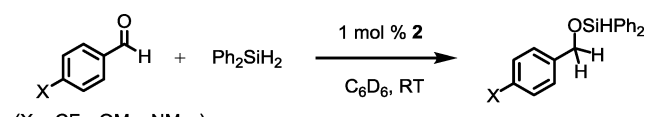


entry ^a	catalyst	conversion; time	yield ^b
1 ^c	$(\text{Ph}^{\text{DPB}}\text{Mes})\text{Ni}$	>98%; 5.9 h	99%
2	1	>99%; <2 min	99%
3	2	>99%; <2 min	99%

^a1 mmol of Ph_2SiH_2 , 1 mmol of benzaldehyde, 5 mol % catalyst, 500 μL of C_6D_6 . ^bDetermined by ^1H NMR integration against an internal FeCp_2 standard. ^cFrom ref 11.

shown rate enhancement with electron-withdrawing substituents.^{11,62,65} Curiously, we found that installing either an electron-withdrawing or electron-donating group led to a dramatic enhancement in the rate of hydrosilylation by **2** with full consumption of the aldehyde in under 2 min when subjected to our standard conditions (Table 2).

Table 2. Substituent Effects on Hydrosilylation of Benzaldehyde by Ph_2SiH_2



entry ^a	X	conversion; time	yield ^b
1	CF_3	>99%; <2 min	88%
2	OMe	>99%; <2 min	95%
3	NMe_2	>99%; <2 min	83%
4	H	>98%; 7.5 h	98%

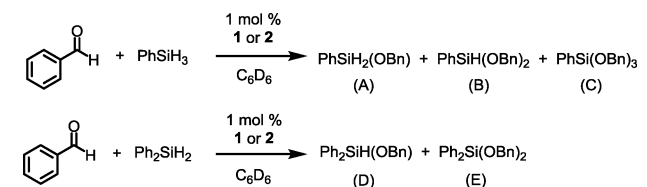
^a1 mmol of Ph_2SiH_2 , 1 mmol of substrate, 1 mol % **2**, 500 μL of C_6D_6 . ^bDetermined by ^1H NMR integration against an internal FeCp_2 standard.

Additional studies showed PhSiH_3 to be competent for hydrosilylation of benzaldehyde. The selectivity for a single hydrosilylation product in this reaction was decreased due to the presence of additional Si–H bonds, which facilitated reduction of multiple benzaldehyde equivalents by a single PhSiH_3 molecule. We also found that at lower catalyst loadings the selectivity for a 1:1 stoichiometry of silane to benzaldehyde was reduced and additional products from the reduction of multiple benzaldehyde equivalents were detected in the ^1H NMR spectra and GC-MS traces of the reaction mixtures (Table 3, products A–E).

The marked enhancement in the rate of hydrosilylation of benzaldehyde by **1** and **2** compared to $(\text{Ph}^{\text{DPB}}\text{Mes})\text{Ni}$ prompted us to investigate whether **1** and **2** would display activity for a larger scope of substrates. While the $(\text{Ph}^{\text{DPB}}\text{Mes})\text{Ni}$ system is limited to benzaldehydes, **1** and **2** are competent precatalysts for the hydrosilylation of benzaldehydes, alkyl aldehydes, and aryl and alkyl ketones (Tables 2, 3, 4).

Increasing the steric bulk about the carbonyl resulted in a decrease in rate, as evidenced on comparing the hydrosilylation of *tert*-butyl methyl ketone to that of 2-pentanone (Table 4 entries 5, 6, 13, 14). We observed rapid hydrosilylation of 2-pentanone by both **1** and **2**, whereas hydrosilylation of *tert*-butyl methyl ketone was sluggish even at elevated temperatures, showing little conversion after 30 h at 50 °C. The hydro-

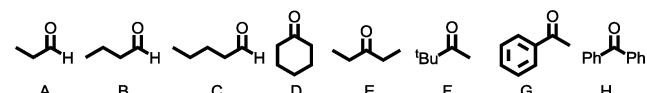
Table 3. Comparison of Primary, Secondary, and Tertiary Silanes in Hydrosilylation of Benzaldehyde



entry ^a	catalyst	silane	conversion (time)	yield ^b
1	1	PhSiH_3	>98% (5.6 h)	0% (A)
				63% (B)
				24% (C)
2	1	Ph_2SiH_2	>97% (10 h)	70% (D)
				19% (E)
				0% (C)
3	2	PhSiH_3	>98% (2 min)	37% (A)
				27% (B)
				0% (C)
4	2	Ph_2SiH_2	>98% (7.5 h)	98% (D)
				0% (E)
				0% (C)

^a1 mmol of silane, 1 mmol of benzaldehyde, 1 mol % catalyst, 500 μL of C_6D_6 . ^bDetermined by ^1H NMR integration against an internal FeCp_2 standard.

Table 4. Summary for Hydrosilylation by Ph_2SiH_2 of Various Aldehydes and Ketones by **1** and **2**

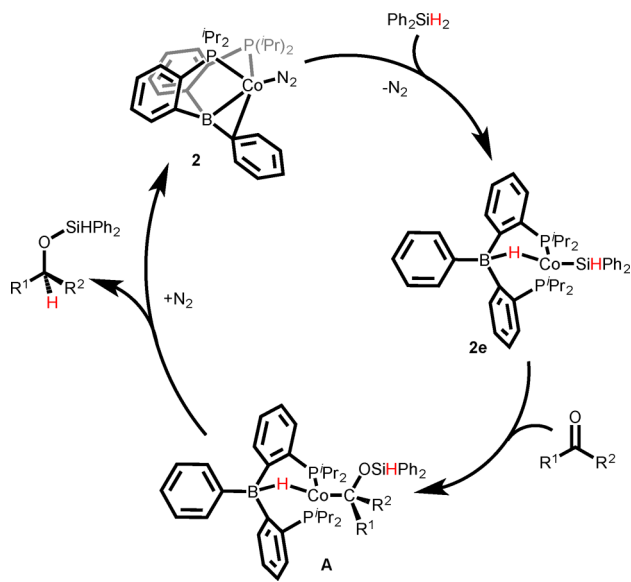


entry ^a	catalyst	substrate	conversion (time)	yield ^c	
1 ^b	1	A	>99%; <5 min	98%	
2 ^b		B	>99%; <10 min	98%	
3 ^b		C	>99%; <10 min	98%	
4 ^b		D	0%; 24 h	0%	
5		E	>98%; 12 min	99%	
6 ^e		F	<1%; 78 h	< 1%	
7		G	>97%; 21.4 h	97%	
8		H	>90%; 18.5 h	86%	
9 ^b		2	A	>99%; <2 min	99%
10			B	>99%; <7 min	99%
11 ^b			C	>98%; <7 min	97%
12 ^b			D	>96%; 99 h	97%
13			E	>99%; 22.4 h	99%
14 ^e			F	17%; 78 h	16%
15			G	>98%; 3.4 h	86%
16			H	>98%; 13 min	84%

^a1 mmol of substrate, 1 mmol of silane, 1 mol % catalyst, 500 μL of C_6D_6 . ^b1 mmol of substrate, 1 mmol of Ph_2SiH_2 , 1 mol % catalysts, 500 μL of 4:1 THF/*d*₈-THF. ^cDetermined by ^1H NMR integration against an internal FeCp_2 standard. ^eReactions were allowed to proceed at room temperature for 48 h followed by heating to 50 °C for 30 h and then worked up.

silylation of benzophenone (a highly activated ketone) proceeds much faster than that of acetophenone despite the increased steric hindrance at the carbonyl.

A plausible mechanistic scenario for the catalytic hydrosilylation of carbonyls by **2** is outlined in Scheme 5. This mechanism is similar to the mechanism we have proposed for catalytic hydrosilylation of benzaldehydes by $(\text{Ph}^{\text{DPB}}\text{Mes})\text{Ni}$, where we were able to spectroscopically observe a borohydrido-siloxy alkyl intermediate during catalytic turnover.¹¹ The

Scheme 5. Possible Catalytic Cycle for Hydrosilylation Mediated by **2**

structural similarity between **2** and $(\text{PhDPB}^{\text{Mes}})\text{Ni}$ may allow for a similar mechanism, although because the Co-catalyzed cycle involves paramagnetic species, it is not as straightforward to identify intermediates as for the $(\text{PhDPB}^{\text{Mes}})\text{Ni}$ system. We nevertheless speculate that the first step in the catalytic cycle is replacement of the N_2 ligand by silane along with Si–H bond activation to give **2e**. Insertion of the ketone into the Co–Si bond would then give a borohydrido-siloxyalkyl intermediate (Scheme 5, A) as demonstrated for $(\text{PhDPB}^{\text{Mes}})\text{Ni}$. Reductive elimination then releases the hydrosilylation product.

It is interesting to note that in almost all cases **2** facilitates the most rapid conversion of the carbonyl to the hydrosilylated product. This contrasts with other reports, comparing isostructural Fe and Co compounds as hydrosilylation catalysts. As an example, Turculet has studied isostructural $(\text{N-PAD})\text{M}(\text{N}(\text{SiMe}_3)_2)$ ($\text{M} = \text{Fe}, \text{Co}$; $\text{N-PAD} = 2,6\text{-diisopropyl-}N\text{-di-tert-butylphosphinoamidinate}$) compounds and demonstrated that the Fe analogues consistently and dramatically outperform the Co system.²⁴ Additionally, the majority of cobalt-catalyzed carbonyl hydrosilylations take place at elevated temperatures and require longer reaction times and greater catalyst loading than those observed in this work.^{22–24,56,60,61} We have prepared and tested several known catalysts under the conditions used herein to accurately compare their performance against **1** and **2**. These data are summarized in Table 5. Li, Klein, and Flörke have reported a Co(III) hydride, $(\text{TSA})\text{Co}(\text{H})(\text{PMe}_3)_3$ (TSA

Table 5. Comparison of Known Catalysts with **1** and **2** for Hydrosilylation of Acetophenone by Ph_2SiH_2

entry ^a	catalyst ^b	conversion; time	yield ^c
1	1	>97%; 21.4 h	97%
2	2	>98%; 3.4 h	86%
3	$\text{Fe}\{\text{N}(\text{SiMe}_3)_2\}_2$	>96%; 0.8 h	100%
4	$\text{Co}\{\text{N}(\text{SiMe}_3)_2\}_2$	26%; 5.2 days	26%
5	$(\text{TSA})\text{Co}(\text{H})(\text{PMe}_3)_3$	15%; 4.1 days	13%

^a1 mmol of acetophenone, 1 mmol of Ph_2SiH_2 , 1 mol % catalyst, 500 μL of C_6D_6 . ^bSee Chart 2. ^cDetermined by ^1H NMR integration against an internal FeCp_2 standard.

= 2-mercaptobenzoyl) (Table 5 entry 4), which achieves a TOF of $\sim 50 \text{ h}^{-1}$ when heated to 40°C or higher.^{23,59} This compound has been cited by Trovitch in a recent perspective as the best reported cobalt catalyst for ketone hydrosilylation.⁵⁹ When tested under identical conditions, **2** significantly outpaces $(\text{TSA})\text{Co}(\text{H})(\text{PMe}_3)_3$; $(\text{TSA})\text{Co}(\text{H})(\text{PMe}_3)_3$ consumes only a fraction of substrate over the course of several days under our standard conditions. To our knowledge **2** is hence the most active cobalt hydrosilylation catalyst for ketones and aldehydes reported to date, at least under the conditions studied herein. An Fe-based catalyst studied by Tilley, however, was also evaluated for comparison under the present conditions and was found to afford full conversion of substrate slightly more rapidly than for **1** or **2** (Table 5, entry 3).²²

CONCLUSION

We have shown that the first-row transition metal–borane compounds **1** and **2** are capable of facilitating a variety of E–H bond activations and are competent precatalysts for the hydrosilylation of ketones and aldehydes. Reactivity with substrates such as PhOH and PhSH proceeded under mild conditions without use of a directing group, giving terminal Fe and Co phenolates, a dimeric Fe-phenylthiolate-borohydride, and a terminal Co phenylthiolate. The reactivity of **1** and **2** with less reactive E–H bonds such as aryl C–H and N–H bonds was facilitated by the use of substrates capable of chelating the metal center. ^1H NMR, X-band EPR, and solution IR studies indicated that reversible activation of the Si–H bonds in diphenylsilane is mediated by **2**, prompting us to investigate **1** and **2** for applications in hydrosilylation catalysis. We found that **1** and **2** are competent precatalysts for the hydrosilylation of aldehydes and ketones under mild conditions, and these catalysts outperform our previously reported and structurally related Ni system. Additionally, when tested under identical conditions against other reported cobalt hydrosilylation catalysts, we found **2** to exhibit the highest catalytic activity. The current study thus highlights the applicability of metal–boranes as precatalysts for hydrosilylation of ketones and aldehydes.

EXPERIMENTAL SECTION

General Considerations. All manipulations were performed using standard Schlenk or glovebox techniques under an atmosphere of N_2 . Solvents were degassed and dried by sparging with N_2 gas and passage through an activated alumina column. Deuterated solvents were purchased from Cambridge Isotopes Laboratories, Inc., and were degassed and stored over activated 3 Å molecular sieves prior to use. Reagents were purchased from commercial vendors and used without further purification unless otherwise noted. Propanal, butanal, pentanal, and cyclohexanone were dried over CaSO_4 , distilled under nitrogen or vacuum, and stored over 3 Å molecular sieves prior to use. All reagents were checked for purity by ^1H NMR spectroscopy prior to use. DPB^{66} and $[(\text{DPB})\text{Fe}]_2(\text{N}_2)^{25}$ were synthesized according to literature procedures. Combustion analyses were performed by Midwest Microlab (Indianapolis, IN, USA) or Robertson Microlit Laboratories (Ledgewood, NJ, USA).

Spectroscopic Measurements. ^1H , ^{13}C , ^{31}P , and ^{11}B NMR spectra were collected at room temperature on a Varian 400 MHz spectrometer or a Varian 300 MHz spectrometer. ^1H and ^{13}C spectra were referenced to residual solvent resonances. ^{31}P NMR spectra were referenced to external 85% phosphoric acid ($\delta = 0 \text{ ppm}$). ^{11}B NMR spectra were referenced to $\text{BF}_3\cdot\text{Et}_2\text{O}$ ($\delta = 0 \text{ ppm}$). UV–vis measurements were performed with a Cary 50 instrument with Cary WinUV software. IR spectra were obtained as thin films formed by evaporation or as a solution using a cell with KBr windows using a

Bruker Alpha Platinum ATR spectrometer with OPUS software. EPR spectra were recorded on a Bruker EMS spectrometer in frozen solutions at 77 K. EPR simulations used the EasySpin software package.⁶⁷

X-ray Crystallography. X-ray diffraction studies were carried out at the Caltech Division of Chemistry and Chemical Engineering X-ray Crystallography Facility on a Bruker three-circle SMART diffractometer with a SMART 1K CCD detector, APEX CCD detector, or Bruker D8 VENTURE Kappa Duo PHOTON 100 CMOS detector. Data were collected at 100 K using Mo $K\alpha$ radiation ($\lambda = 0.71073 \text{ \AA}$) or Cu $K\alpha$ radiation ($\lambda = 1.54178 \text{ \AA}$). Structures were solved by direct or Patterson methods using SHELXS and refined against F^2 on all data by full-matrix least-squares with SHELXL-97.⁶⁸ All non-hydrogen atoms were refined anisotropically. With the exception of any $\mu\text{-B-H-M}$ hydrides that were located on the difference map, all hydrogen atoms were placed at geometrically calculated positions and refined using a riding model. The isotropic displacement parameters of all hydrogen atoms were fixed at 1.2 (1.5 for methyl groups) times the U_{eq} of the atoms to which they are bonded. An A level alert is generated by Checkcif for the structure of **1d** because of a close H–H contact between H20C (a calculated isopropyl methyl hydrogen) and H108 (a calculated aryl H atom on the minor part of the disordered 8-amidoquinolinyl ligand). Because the close H–H contact is between a calculated methyl H atom and a partially occupied calculated H atom on a highly disordered ligand, we do not anticipate that this is cause for concern or indicative of missing symmetry or a false solution.

Preparation of (DPB)FeOPh (1a). A 62.7 mg (0.058 mmol) amount of **1** was dissolved in ca. 10 mL of benzene to form a dark red-brown solution. A 10.8 mg (0.115 mmol) amount of PhOH dissolved in ca. 5 mL of benzene was added to the solution of **1**. Over the course of ~1.5 h the solution turned from dark red-brown to dark yellow-brown. The solution was allowed to stir overnight (~16 h). GC analysis of the headspace of the reaction mixture showed formation of H_2 . The reaction mixture was lyophilized, leaving a dark residue. Crystals suitable for X-ray diffraction studies were grown by cooling a concentrated solution in Et_2O to $-30 \text{ }^\circ\text{C}$ in a freezer. Yield: 71.1 mg (0.114 mmol), 99.1%. $^1\text{H NMR}$ (400 MHz, C_6D_6): δ 142.34, 109.34, 91.02, 70.19, 5.63, 39.49, 28.01, 21.49, 21.15, 12.18, 11.02, 5.20, -0.14 , -0.26 , -5.69 , -6.69 , -11.02 , -13.75 , -16.56 , -18.12 , -28.44 , -36.17 , -52.16 . Solution magnetic moment (25 $^\circ\text{C}$, C_6D_6): $3.9 \mu_{\text{B}}$. UV–vis [toluene, $\lambda(\text{nm})\{\epsilon(\text{M}^{-1} \text{cm}^{-1})\}$]: 318(sh){5723}, 393{3434}, 877{219}. Combustion analysis for $\text{C}_{36}\text{H}_{46}\text{BFeOP}_2$: calcd C 69.36, H 7.44; found C 69.25, H 7.03.

Alternative Synthesis of 1a. A 17.9 mg (0.03 mmol) sample of (DPB)FeBr was dissolved in 10 mL of Et_2O , and the mixture was added to a solution of 3.7 mg (0.03 mmol) of NaOPh in 5 mL of Et_2O and stirred for 16 h. The resulting yellow-brown solution was filtered through Celite and evaporated to dryness, leaving a brown residue. This residue was extracted in benzene and lyophilized, giving a fine brown powder, which showed identical spectroscopic features to the product **1a** prepared by the previously described method. Yield: 17.4 mg (0.028 mmol), 93.3%.

Preparation of [(DPBH)Fe(SPh)]₂ (1b). A 116.3 mg (0.107 mmol) portion of **1** was dissolved in ca. 10 mL of benzene to form a dark red-brown solution. Then 23.6 mg (0.0214 mmol) of PhSH dissolved in ca. 5 mL of benzene was added to the solution of **1**. Over the course of ~1.5 h the solution turned from dark red-brown to red-orange. The solution was allowed to stir overnight and lyophilized, leaving a fine pale orange powder. Yield: 105.2 mg (0.0821 mmol), 76.7%. $^1\text{H NMR}$ (400 MHz, C_6D_6): δ 117.20, 52.99, 48.53, 42.05, 24.28, 13.75, 13.53, 9.11, -7.71 , -8.62 , -15.94 , -21.91 , -24.23 , -25.02 , -27.25 , -44.97 . Solution magnetic moment (25 $^\circ\text{C}$, toluene- d_6): $4.77 \mu_{\text{B}}$ per Fe center. IR (thin film from C_6D_6 , cm^{-1}): 1961 (br, B–H–Fe). UV–vis [toluene, $\lambda(\text{nm})\{\epsilon(\text{M}^{-1} \text{cm}^{-1})\}$]: 324(sh){9600}, 418(sh){3200}. Combustion analysis for $\text{C}_{72}\text{H}_{94}\text{B}_2\text{Fe}_2\text{S}_2\text{P}_4$: calcd C 67.52, H 7.40; found C 66.85, H 6.95.

Preparation of (DPBH)Fe(benzo[h]quinolin-10-yl) (1c). A solution of **1** (19.1 mg, 0.0176 mmol) and benzo[h]quinoline (6.3 mg, 0.035 mmol) in 0.7 mL of C_6D_6 was heated at 70 $^\circ\text{C}$ until all of **1** was consumed (3 h). Solvent was removed *in vacuo*, and the resulting

solids were washed with cold pentane ($3 \times 1 \text{ mL}$) and dissolved in minimal Et_2O . Evaporation of the saturated Et_2O solution into HMDSO gave single crystals of **1c**, which were lyophilized from C_6H_6 to give magenta solids. Yield: 14.0 mg (0.0197 mmol), 56%. $^1\text{H NMR}$ (500 MHz, C_6D_6): δ 9.02–8.86 (m, 1H), 7.56 (d, $^3J_{\text{HH}} = 8.7 \text{ Hz}$, 1H), 7.47 (d, $^3J_{\text{HH}} = 7.9 \text{ Hz}$, 2H), 7.46 (s, 1H), 7.45–7.41 (m, 4H), 7.39 (d, $^3J_{\text{HH}} = 6.6 \text{ Hz}$, 2H), 7.33–7.28 (m, 4H), 7.25–7.19 (m, 4H), 7.12 (s, 1H), 6.70 (d, $^3J_{\text{HH}} = 5.3 \text{ Hz}$, 1H), 6.41 (dd, $^3J_{\text{HH}} = 7.8$, 5.4 Hz, 1H), 1.78–1.50 (m, 4H), 0.87 (d, $^3J_{\text{HH}} = 7.0 \text{ Hz}$, 6H), 0.73 (d, $^3J_{\text{HH}} = 6.3 \text{ Hz}$, 6H), 0.18 (s, 6H), 0.11 (d, $^3J_{\text{HH}} = 6.4 \text{ Hz}$, 6H), -22.80 (s, 1H). $^{11}\text{B NMR}$ (160 MHz, C_6D_6): δ -7.29 . $^{13}\text{C NMR}$ (126 MHz, C_6D_6): δ 160.71, 153.81, 153.63, 147.23, 146.58, 144.03, 135.36, 132.95, 129.87, 129.67, 128.44, 126.20, 125.03, 124.62, 124.41, 122.23, 119.20, 116.80, 26.57, 23.35, 20.97, 18.75, 18.49, 18.36. $^{31}\text{P NMR}$ (202 MHz, C_6D_6): δ 41.26. IR (thin film from C_6D_6 , cm^{-1}): 2279, 2270 (B–H–Fe). UV–vis [toluene, $\lambda(\text{nm})\{\epsilon(\text{M}^{-1} \text{cm}^{-1})\}$]: 287(sh){26,608}, 346(sh){5765}, 366{7761}, 421(sh){3548}, 498{5543}, 537(sh){5211}. Combustion analysis for $\text{C}_{43}\text{H}_{50}\text{BFenP}_2$: calcd C 72.80, H 7.10, N 1.97; found C 72.51, H 6.84, N 1.84.

Preparation of (DPBH)Fe(8-amidoquinoline) (Mixture of Two Isomers) (1d). A solution of **1** (17.4 mg, 0.0160 mmol) and 8-aminoquinoline (4.6 mg, 0.032 mmol) in 0.7 mL of C_6D_6 was allowed to stand at RT until all **1** was consumed (~1 h). Volatiles were removed *in vacuo*, and the resulting solids were washed with cold pentane ($3 \times 1 \text{ mL}$) and dissolved in minimal Et_2O . Evaporation of the saturated Et_2O solution into hexamethyldisiloxane (HMDSO) furnished crystals of **1d**, which were lyophilized to give a red powder. Yield: 18.0 mg (0.027 mmol), 83%. $^1\text{H NMR}$ (300 MHz, C_6D_6): δ 141.88, 103.99, 85.33, 83.94, 77.91, 72.22, 68.70, 58.27, 57.69, 51.90, 24.40, 22.51, 19.91, 17.52, 17.18, 15.04, 14.47, 12.77, 11.31, 2.17, 0.74, -1.81 , -3.85 , -7.08 , -9.09 , -9.45 , -12.79 , -15.24 , -20.90 , 25.02, -33.79 , -81.35 , -83.00 , -84.84 , -103.43 . Solution magnetic moment (25 $^\circ\text{C}$, C_6D_6): $5.2 \mu_{\text{B}}$. IR (thin film from C_6D_6 , cm^{-1}): 3373 (N–H), 2130 (br, s, B–H–Fe for isomer A), 2000 (B–H–Fe for isomer B). UV–vis [toluene, $\lambda(\text{nm})\{\epsilon(\text{L mol}^{-1} \text{cm}^{-1})\}$]: 297{14 527}, 368(sh){5188}, 415(sh){3761}, 514{2931}. Combustion analysis for $\text{C}_{39}\text{H}_{49}\text{BFenN}_2\text{P}_2$: calcd C 69.45, H 7.32, N 4.15; found C 68.55, H 7.09, N 3.94.

Preparation of (DPB)Co(N₂) (2). A solution of 0.8483 g (1.79 mmol) of DPB and 0.2316 g (1.78 mmol) of CoCl_2 in tetrahydrofuran (ca. 80 mL) was stirred until no solids remained, leaving a deep blue solution. Solvent was removed *in vacuo*, and the remaining blue residue was triturated in Et_2O for 15 min. Solvent was removed *in vacuo*, and the blue residue was dissolved in benzene (80 mL). Freshly prepared 1% sodium mercury amalgam (0.0864 g of Na, 3.76 mmol) was added to the dark blue solution and stirred vigorously for 24 h. The resulting dark red-orange solution was decanted and filtered through Celite. Lyophilization afforded a fine dark brown powder. This powder was dissolved in minimal Et_2O and cooled in a freezer to $-30 \text{ }^\circ\text{C}$, affording red-orange crystals of **2**. Yield: 0.850 g (1.51 mmol), 84%. $^1\text{H NMR}$ (400 MHz, C_6D_6): δ 17.79, 14.77, 4.04, 2.42, -2.74 , -4.04 . Solution magnetic moment (25 $^\circ\text{C}$, C_6D_6): $1.8 \mu_{\text{B}}$. IR (thin film from C_6D_6 , cm^{-1}): 2098 (N_2). UV–vis [toluene, $\lambda(\text{nm})\{\epsilon(\text{M}^{-1} \text{cm}^{-1})\}$]: 288{9346}. Combustion analysis for $\text{C}_{30}\text{H}_{41}\text{BCoN}_2\text{P}_2$ was consistently low in nitrogen and high in carbon and hydrogen, consistent with the labile N_2 ligand; a representative analysis is shown: calcd C 64.19, H 7.36, N 4.99; found C 64.52, H 7.57, N 4.13.

Preparation of (DPB)CoBr (2-Br). A 57.1 mg (0.12 mmol) sample of DPB was dissolved in 10 mL of THF with 26.4 mg (0.12 mmol) of CoBr_2 , giving a clear blue solution. A dark red-orange solution of **2**, 67.6 mg (0.12 mmol), dissolved in 10 mL of THF was added to the stirring solution of DPB and CoBr_2 via pipet, resulting in darkening of the reaction mixture. After stirring for 16 h the solution was yellow-brown. The reaction mixture was filtered through Celite, and volatiles were removed *in vacuo*, leaving a dark brown residue. The residue was extracted in pentane and filtered through Celite, removing some blue and green solids. The brown pentane extract was evaporated to dryness and dissolved in minimal THF. Large brown crystals of **2-Br** were grown by vapor diffusion of a concentrated THF solution into HMDSO. Crystals of suitable quality for X-ray diffraction were grown

by vapor diffusion of Et₂O into HMDSO. Yield: 134.8 mg (0.22 mmol), 91.7%. ¹H NMR (400 MHz, C₆D₆): δ 21.61, 19.58, 16.11, 6.45, 3.82, 2.80, -1.51, -2.09, -6.81, -9.61, -16.16, -40.72. Solution magnetic moment (25 °C, C₆D₆): 3.0 μ_B. UV-vis [toluene, λ(nm){ε(M⁻¹ cm⁻¹)}]: 353{5713}, 404(sh){2863}. Combustion analysis for C₃₀H₄₁BCoP₂Br: calcd C 58.57, H 6.61; found C 58.76, H 6.74.

Preparation of (DPB)CoOPh (2a). A Schlenk tube was charged with 62.4 mg (0.111 mmol) of **2**, 10.5 mg (0.112 mmol) of PhOH, and C₆H₆ (15 mL), and the mixture was stirred for 16 h at room temperature. A color change from red-orange to orange-brown was observed after overnight stirring. GC analysis of the headspace of the reaction mixture showed formation of H₂. The solution was lyophilized, leaving a fine orange-brown powder. Yield: 63.0 mg (0.1 mmol), 90%. ¹H NMR (400 MHz, C₆D₆): δ 58.44, 34.48, 20.37, 19.82, 18.26, 16.38, 15.53, 5.76, 5.39, -3.26, -4.22, -5.48, -6.83, -7.71, -16.92, -18.67, -19.09, -21.05, -21.44, -46.23, -193.33. Solution magnetic moment (25 °C, C₆D₆): 3.2 μ_B. UV-vis [toluene, λ(nm){ε(M⁻¹ cm⁻¹)}]: 287(sh){13 046}, 425{3346}. Combustion analysis for C₃₆H₄₆BCoP₂: calcd C 69.02, H 7.40; found C 68.14, H 7.46.

Alternative Synthesis of 2a. A 21.9 mg (0.036 mmol) amount of (DPB)CoBr was combined with 4.2 mg (0.036 mmol) of NaOPh in ~10 mL of THF, and the mixture was stirred for 16 h. The resulting orange-brown solution was filtered through Celite, and volatiles were removed *in vacuo*. The resulting residue was extracted in benzene and lyophilized, giving a fine orange-brown powder with spectroscopic features identical to **2a** prepared by the previously described method. Yield: 20.9 mg (0.033 mmol), 91.7%.

Preparation of (DPB)CoSPh (2b). A 64.2 mg (0.114 mmol) amount of **2** and 12.6 mg (0.114 mmol) of PhSH were dissolved in benzene (15 mL) in a Schlenk tube, and the mixture was stirred for 16 h at room temperature. The solution color changed from dark red-orange to deep red. GC analysis of the headspace of the reaction mixture showed formation of H₂. The reaction mixture was lyophilized, leaving a dark red powder, which was then dissolved in minimal Et₂O. Crystals suitable for X-ray diffraction studies were obtained by vapor diffusion of an Et₂O solution into HMDSO. Yield: 73.5 mg (0.114 mmol), 100%. ¹H NMR (400 MHz, C₆D₆): δ 184.19, 25.53, 20.79, 15.72, 15.16, 14.22, 13.39, 10.08, 9.77, 5.66, 4.67, 3.05, 1.67, -0.92, -1.09, -1.96, -2.45, -12.17, -17.10, -19.90, -46.22. Solution magnetic moment (25 °C, toluene-*d*₆): 2.6 μ_B. UV-vis [toluene, λ(nm){ε(L mol⁻¹ cm⁻¹)}]: 283(sh){18 858}, 355(sh){3705}, 478{3821}. Combustion analysis for C₃₆H₄₆BCoNP₂: calcd C 67.19, H 7.36; found C 66.97, H 7.09.

Alternative Synthesis of 2b. A 19.6 mg (0.032 mmol) portion of **2-Br** was combined with 4.2 mg (0.032 mmol) of NaSPh in 10 mL of THF, and the mixture was stirred for 16 h. The resulting deep red solution was filtered through Celite, and the volatiles were removed *in vacuo*, giving a dark red residue. This residue was extracted in benzene and lyophilized, giving a fine red powder with spectroscopic features identical to **2b** prepared by the previously described method. Yield: 19.4 mg (0.030 mmol), 90.9%.

Preparation of (DPBH)Co(benzo[h]quinolin-10-yl), 2c. A 200.0 mg (0.356 mmol) amount of **2** and 64.1 mg (0.357 mmol) of benzo[h]quinoline were dissolved in ca. 25 mL of benzene in a Schlenk tube. The solution was freeze-pump-thawed for 3 × 15 min cycles to remove N₂ and heated to 60 °C for 24 h, turning from dark red-orange to bright red-orange. The solution was lyophilized, leaving a red-orange solid. Dissolving this solid in minimal Et₂O and cooling to -30 °C afforded crystals of **2c** suitable for X-ray diffraction studies. Yield: 123.5 mg (0.173 mmol), 48.6%. ¹H NMR (300 MHz, C₆D₆): δ 19.05, 15.79, 10.47, 8.91, 5.49, 3.36, -1.38. Solution magnetic moment (25 °C, C₆D₆): 1.8 μ_B. IR (thin film, C₆D₆): 2047 cm⁻¹ (B-H-Co). UV-vis [toluene, λ(nm){ε(L mol⁻¹ cm⁻¹)}]: 378{3913}, 406{3563}, 431{3682}, 454{3800}. Combustion analysis for C₄₃H₅₀BCoNP₂: calcd C 72.48, H 7.07, N 1.97; found C 72.23, H 6.78, N 1.94.

Preparation of (DPBH)Co(8-amidoquinoline), 2d. A 16.1 mg (0.029 mmol) sample of **2** and 4.2 mg (0.029 mmol) of 8-aminoquinoline were dissolved in benzene (ca. 15 mL), and the mixture was freeze-

pump-thawed for 3 × 15 min cycles to remove N₂. The solution turned from deep red-orange to deep purple after stirring for 24 h. The reaction mixture was lyophilized, giving a dark purple solid, which was dissolved in minimal Et₂O and cooled in a freezer to -30 °C, affording purple crystals of **2d**. Yield: 17.2 mg (0.025 mmol), 86.2%. ¹H NMR (300 MHz, C₆D₆): δ 37.30, 18.47, 8.99, 8.29, 7.60, 6.52, 5.43, 3.49, 1.86, -0.87. Solution magnetic moment (25 °C, C₆D₆): 2.4 μ_B. IR (thin film, C₆D₆): 1961 cm⁻¹ (B-H-Co), 3384 cm⁻¹ (N-H), 3478 cm⁻¹ (N-H). UV-vis [toluene, λ(nm){ε(L mol⁻¹ cm⁻¹)}]: 342(sh){3874}, 409(sh){2325}, 545{3390}. Combustion analysis for C₃₉H₄₉BCoN₂P₂: calcd C 69.14, H 7.29, N 4.13; found C 68.82, H 7.14, N 4.04.

Generation of (DPBH)Co(SiHPh₂), 2e. A 6.7 mg (0.012 mmol) amount of **2** was dissolved in 0.5 mL of C₆D₆, and this was combined with neat Ph₂SiH₂ (220 mg, 1.2 mmol). The solution was divided into two aliquots (0.35 and 0.15 mL) and loaded into an EPR tube and an NMR tube equipped with J-Young gas addition fittings. The EPR and NMR tubes were subjected to three freeze-pump-thaw cycles on a Schlenk line to generate a mixture of the S = 1/2 species **2e** observed by ¹H NMR and X-band EPR and some unidentified diamagnetic impurities. For **2e**: ¹H NMR (400 MHz, C₆D₆): δ 22.44, 20.43, 16.24, 16.12, 16.00, -0.63, -2.10, -3.90, -5.57, -7.76, -9.69, -11.56, -12.47, -15.76, -40.35, -40.84, -41.11. IR (solution in C₆H₆ with 100 equiv of Ph₂SiH₂): 1810 cm⁻¹ (B-H-Co). For impurities: ¹H NMR (400 MHz, C₆D₆): δ -17.13 (t) (J_{P-H} = 44.3 Hz). ³¹P NMR (162 MHz, C₆D₆): δ 77.96, 58.73, 57.66.

Hydrosilylation Catalytic Protocol. In a typical experiment a J-Young NMR tube was loaded with a 0.005 mmol (100 μL, 0.05 M) solution of **1** in C₆D₆ or a 0.01 mmol (100 μL, 0.1 M) solution of **2** in C₆D₆, a 100 μL FeCp₂ solution in C₆D₆ (0.355 M), and 300 μL of C₆D₆ (total volume 500 μL). The tube was then frozen in a cold well cooled by liquid nitrogen. The frozen tube was loaded with 185.8 μL of Ph₂SiH₂ (1.0 mmol) and 1.0 mmol of aldehyde or ketone, sealed, and kept frozen. The frozen tube was rapidly thawed at the NMR spectrometer, shaken vigorously, and monitored by ¹H NMR spectroscopy until all starting materials had been consumed. After completion the reaction mixture was exposed to air, diluted with CH₂Cl₂, filtered through a plug of silica, and analyzed by GC-MS. Hydrosilylation products were identified by comparison of the ¹H NMR spectra and GC-MS traces to those reported in the literature.^{11,22,63,69,70} To aid characterization, (1-(4-trifluoromethylphenyl)methoxy)diphenylsilane was converted to 4-(trifluoromethyl)phenyl methanol by treatment with 1 M HCl; the ¹H NMR and GC-MS data obtained agree with the literature data.⁷¹ Reactions run in the absence of FeCp₂ showed the same distribution of products by ¹H NMR and GC-MS and reached completion in the same amount of time. Control experiments showed little to no reaction of PhSiH₃ or Ph₂SiH₂ with substrates in the absence of **1** or **2** in the time frame in which the catalyzed reaction occurs.

Mercury Drop Test for Homogeneity. A solution of either 0.005 mmol of **1** or 0.01 mmol of **2** in benzene (500 μL) was stirred over excess Hg metal (173–200 equiv) for 15 min at 25 °C. Benzaldehyde (102 μL, 1.0 mmol) was added to the stirring solution followed by Ph₂SiH₂ (185.8 μL, 1.0 mmol), and the mixture was stirred. ¹H NMR and GC-MS analysis of the reaction mixtures showed full conversion of starting materials into products in the expected time.

■ ASSOCIATED CONTENT

● Supporting Information

The Supporting Information is available free of charge on the ACS Publications website at DOI: 10.1021/acs.organomet.5b00530.

Experimental parameters for X-ray crystallographic studies, additional figures, ¹H NMR data, additional EPR spectra, EPR simulation parameters (PDF)

Cif file (CIF)

AUTHOR INFORMATION

Corresponding Author

*E-mail: jpeters@caltech.edu.

Notes

The authors declare no competing financial interest.

ACKNOWLEDGMENTS

The authors would like to acknowledge the financial support provided by the NSF Center for Chemical Innovation (CCI; CHE-1305124) and the Gordon and Betty Moore Foundation. The authors thank Dr. Michael Takase and Lawrence Henling at the Caltech X-ray crystallographic facility for assistance with XRD studies. The authors also thank Dr. Tzu-Pin Lin for editorial assistance and insightful suggestions.

DEDICATION

This contribution is dedicated to the fond memory of Professor Gregory L. Hillhouse.

REFERENCES

- (1) Crabtree, R. H. *The Organometallic Chemistry of the Transition Metals*, 5th ed.; John Wiley & Sons Inc.: New York, 2009.
- (2) Miessler, G. L.; Tarr, D. A. *Inorganic Chemistry*, 4th ed.; Prentice Hall: New York, 2011.
- (3) Ojima, I.; Kogure, T.; Kumagai, M.; Horiuchi, S.; Sato, T. *J. Organomet. Chem.* **1976**, *122*, 83–97.
- (4) Zheng, G. Z.; Chan, T. H. *Organometallics* **1995**, *14*, 70–79.
- (5) *Catalysis without Precious Metals*; Bullock, R. M., Ed.; Wiley-VCH Verlag GmbH & Co. KGaA: Weinheim, Germany, 2010.
- (6) Hu, X. *Chem. Sci.* **2011**, *2*, 1867–1886.
- (7) Owen, G. R. *Chem. Soc. Rev.* **2012**, *41*, 3535–3546.
- (8) Devillard, M.; Bouhadir, G.; Bourissou, D. *Angew. Chem., Int. Ed.* **2015**, *54*, 730–732.
- (9) Harman, W. H.; Peters, J. C. *J. Am. Chem. Soc.* **2012**, *134*, 5080–5082.
- (10) Fong, H.; Moret, M.-E.; Lee, Y.; Peters, J. C. *Organometallics* **2013**, *32*, 3053–3062.
- (11) MacMillan, S. N.; Hill Harman, W.; Peters, J. C. *Chem. Sci.* **2014**, *5*, 590–597.
- (12) Chapman, A. M.; Haddow, M. F.; Wass, D. F. *J. Am. Chem. Soc.* **2011**, *133*, 18463–18478.
- (13) Bonanno, J. B.; Henry, T. P.; Wolczanski, P. T.; Pierpont, A. W.; Cundari, T. R. *Inorg. Chem.* **2007**, *46*, 1222–1232.
- (14) (a) Stephan, D. W.; Erker, G. *Angew. Chem., Int. Ed.* **2010**, *49*, 46–76. (b) Stephan, D. W.; Erker, G. *Angew. Chem., Int. Ed.* **2015**, *54*, 6400–6441.
- (15) Harman, W. H.; Lin, T. P.; Peters, J. C. *Angew. Chem., Int. Ed.* **2014**, *53*, 1081–1086.
- (16) Frank, N.; Hanau, K.; Langer, R. *Inorg. Chem.* **2014**, *53*, 11335–11343.
- (17) Figueroa, J. S.; Melnick, J. G.; Parkin, G. *Inorg. Chem.* **2006**, *45*, 7056–7058.
- (18) Pang, K.; Tanski, J. M.; Parkin, G. *Chem. Commun.* **2008**, 1008–1010.
- (19) Tsoureas, N.; Kuo, Y.-Y.; Haddow, M. F.; Owen, G. R. *Chem. Commun.* **2011**, *47*, 484–486.
- (20) Cowie, B. E.; Emslie, D. J. H. *Chem. - Eur. J.* **2014**, *20*, 16899–16912.
- (21) Barnett, B. R.; Moore, C. E.; Rheingold, A. L.; Figueroa, J. S. *J. Am. Chem. Soc.* **2014**, *136*, 10262–10265.
- (22) Yang, J.; Tilley, T. D. *Angew. Chem., Int. Ed.* **2010**, *49*, 10186–10188.
- (23) Niu, Q.; Sun, H.; Li, X.; Klein, H. F.; Flörke, U. *Organometallics* **2013**, *32*, 5235–5238.
- (24) Ruddy, A. J.; Kelly, C. M.; Crawford, S. M.; Wheaton, C. A.; Sydora, O. L.; Small, B. L.; Stradiotto, M.; Turculet, L. *Organometallics* **2013**, *32*, 5581–5588.
- (25) Suess, D. L. M.; Peters, J. C. *J. Am. Chem. Soc.* **2013**, *135*, 4938–4941.
- (26) Suess, D. L. M.; Peters, J. C. *J. Am. Chem. Soc.* **2013**, *135*, 12580–12583.
- (27) The position of the bridging H atom could not be reliably located and refined upon.
- (28) Hayashi, Y.; Yamamoto, T.; Yamamoto, A.; Komiya, S.; Kushi, Y. *J. Am. Chem. Soc.* **1986**, *108*, 385–391.
- (29) Archibald, S. J.; Foxon, S. P.; Freeman, J. D.; Hobson, J. E.; Perutz, R. N.; Walton, P. H. *J. Chem. Soc., Dalton. Trans.* **2002**, 2797–2799.
- (30) Buzzeo, M. C.; Iqbal, A. H.; Long, C. M.; Millar, D.; Patel, S.; Pellow, M. A.; Saddoughi, S. A.; Smenton, A. L.; Turner, J. F. C.; Wadhawan, J. D.; Compton, R. G.; Golen, J. A.; Rheingold, A. L.; Doerrer, L. H. *Inorg. Chem.* **2004**, *43*, 7709–7725.
- (31) Mautz, J.; Huttner, G. *Eur. J. Inorg. Chem.* **2008**, *2008*, 1423–1434.
- (32) Jiao, G.; Li, X.; Sun, H.; Xu, X. *J. Organomet. Chem.* **2007**, *692*, 4251–4258.
- (33) Wei, G.; Huang, Z.; Lei, X.; Cao, R.; Jiang, F.; Hong, M.; Liu, H. *Acta Crystallogr., Sect. C: Cryst. Struct. Commun.* **1992**, *48*, 2130–2132.
- (34) Vastag, S.; Markó, L.; Rheingold, A. L. *J. Organomet. Chem.* **1990**, *397*, 231–238.
- (35) Mock, M. T.; Potter, R. G.; O'Hagan, M. J.; Camaioni, D. M.; Dougherty, W. G.; Kassel, W. S.; DuBois, D. L. *Inorg. Chem.* **2011**, *50*, 11914–11928.
- (36) Norinder, J.; Matsumoto, A.; Yoshikai, N.; Nakamura, E. *J. Am. Chem. Soc.* **2008**, *130*, 5858–5859.
- (37) Klein, H.-F.; Camadanli, S.; Beck, R.; Leukel, D.; Flörke, U. *Angew. Chem., Int. Ed.* **2005**, *44*, 975–977.
- (38) Baker, M. V.; Field, L. D. *J. Am. Chem. Soc.* **1986**, *108*, 7433–7434.
- (39) Addison, A. W.; Rao, T. N.; Reedijk, J.; van Rijn, J.; Verschoor, G. C. *J. Chem. Soc., Dalton Trans.* **1984**, 1349–1356.
- (40) Schaad, D. R.; Landis, C. R. *J. Am. Chem. Soc.* **1990**, *112*, 1628–1629.
- (41) Fox, D. J.; Bergman, R. G. *J. Am. Chem. Soc.* **2003**, *125*, 8984–8985.
- (42) Ding, Z.; Yoshikai, N. *Beilstein J. Org. Chem.* **2012**, *8*, 1536–1542.
- (43) Zhang, R.; Zhu, L.; Liu, G.; Dai, H.; Lu, Z.; Zhao, J.; Yan, H. *J. Am. Chem. Soc.* **2012**, *134*, 10341–10344.
- (44) Zhang, Z.; Sun, H.; Xu, W.; Li, X. *Polyhedron* **2013**, *50*, 571–575.
- (45) Ko, J.; Kang, S.; Uhm, J.-K. *Bull. Korean Chem. Soc.* **1994**, *15*, 1122–1124.
- (46) Nishiyama, H. In *Comprehensive Chirality*; Carreira, E. M.; Yamamoto, H., Eds.; Elsevier: Amsterdam, 2012; pp 318–333.
- (47) Riener, K.; Högerl, M. P.; Gigler, P.; Kühn, F. E. *ACS Catal.* **2012**, *2*, 613–621.
- (48) Yamamoto, K.; Hayashi, T. In *Transition Metals for Organic Synthesis*; Beller, M.; Bolm, C., Eds.; Wiley-VCH Verlag GmbH: Weinheim, Germany, 2008; pp 167–191.
- (49) Scheuermann, M. L.; Semproni, S. P.; Pappas, I.; Chirik, P. J. *Inorg. Chem.* **2014**, *53*, 9463–9465.
- (50) Frogneux, X.; Jacquet, O.; Cantat, T. *Catal. Sci. Technol.* **2014**, *4*, 1529–1533.
- (51) Jaseer, E. A.; Akhtar, M. N.; Osman, M.; Al-Shammari, A.; Oladipo, H. B.; Garces, K.; Fernandez-Alvarez, F. J.; Al-Khattaf, S.; Oro, L. A. *Catal. Sci. Technol.* **2015**, *5*, 274–279.
- (52) Iglesias, M.; Fernández-Alvarez, F. J.; Oro, L. A. *ChemCatChem* **2014**, *6*, 2486–2489.
- (53) Aresta, M. In *Activation of Small Molecules*; Tolman, W. B., Ed.; Wiley-VCH Verlag GmbH & Co. KGaA: Weinheim, Germany, 2006; pp 1–35.

- (54) Windle, C. D.; Perutz, R. N. *Coord. Chem. Rev.* **2012**, *256*, 2562–2570.
- (55) Schneider, J.; Jia, H.; Muckerman, J. T.; Fujita, E. *Chem. Soc. Rev.* **2012**, *41*, 2036–2051.
- (56) Inagaki, T.; Phong, L. T.; Furuta, A.; Ito, J.-i.; Nishiyama, H. *Chem. - Eur. J.* **2010**, *16*, 3090–3096.
- (57) Zuo, Z.; Sun, H.; Wang, L.; Li, X. *Dalton Trans.* **2014**, *43*, 11716–11722.
- (58) Zhao, H.; Sun, H.; Li, X. *Organometallics* **2014**, *33*, 3535–3539.
- (59) Trovitch, R. J. *Synlett* **2014**, *25*, 1638–1642.
- (60) Sauer, D. C.; Wadepohl, H.; Gade, L. H. *Inorg. Chem.* **2012**, *51*, 12948–12958.
- (61) Brunner, H.; Amberger, K. J. *Organomet. Chem.* **1991**, *417*, C63–C65.
- (62) Bullock, R. M. In *Catalysis without Precious Metals*; Bullock, R. M., Ed.; Wiley-VCH Verlag GmbH & Co. KGaA: Weinheim, Germany, 2010; pp 51–81.
- (63) Tondreau, A. M.; Lobkovsky, E.; Chirik, P. J. *Org. Lett.* **2008**, *10*, 2789–2792.
- (64) Gallego, D.; Inoue, S.; Blom, B.; Driess, M. *Organometallics* **2014**, *33*, 6885–6897.
- (65) Sui-Seng, C.; Freutel, F.; Lough, A. J.; Morris, R. H. *Angew. Chem., Int. Ed.* **2008**, *47*, 940–943.
- (66) Bontemps, S.; Gornitzka, H.; Bouhadir, G.; Miqueu, K.; Bourissou, D. *Angew. Chem., Int. Ed.* **2006**, *45*, 1611–1614.
- (67) Stoll, S.; Schweiger, A. *J. Magn. Reson.* **2006**, *178*, 42–55.
- (68) Sheldrick, G. M. *SHELXTL 2000*; Universität Göttingen: Göttingen, Germany, 2000.
- (69) Wei, Y.; Han, S.; Kim, J.; Soh, S.; Grzybowski, B. A. *J. Am. Chem. Soc.* **2010**, *132*, 11018–11020.
- (70) Igarashi, M.; Matsumoto, T.; Sato, K.; Ando, W.; Shimada, S. *Chem. Lett.* **2014**, *43*, 429–431.
- (71) Nagendra, G.; Madhu, C.; Vishwanatha, T. M.; Sureshbabu, V. *Tetrahedron Lett.* **2012**, *53*, 5059–5063.